Available online at www.sciencedirect.com

ScienceDirect

Energy Procedia 77 (2015) 271 – 278

Energy Procedia

5th International Conference on Silicon Photovoltaics, SiliconPV 2015

All-screen-printed dopant paste interdigitated back contact solar cell

Giuseppe Scardera, Daniel Inns, Gonghou Wang, Shannon Dugan, Jeffrey Dee, Thomas Dang, Karim Bendimerad, Francesco Lemmi, and Homer Antoniadis

DuPont Silicon Valley Technology Center, 965 E Arques Ave, Sunnyvale, California 94085, USA

Abstract

We report results on the development of a cost-effective all-screen-printed interdigitated back contact (IBC) solar cell process. The rear side interdigitated doping pattern is achieved using screen printed n-type and p-type dopant pastes, and thermal drive-in. Our process provides excellent spatial definition of the doping pattern necessary for fabrication of an IBC solar cell. The doping approach used in this work overcomes limitations associated with conventional pastes, notably poor lateral doping control and reduced bulk lifetime. We demonstrate that wafer lifetime remains high, well above 1.5 msec, at the end of the solar cell process, enabling high cell efficiencies. Contacts are also achieved using screen printed fire-through metal pastes. We present pilot line data for n-type CZ silicon, 156 mm pseudo-square cells achieving just over 21% efficiency.

Peer review by the scientific conference committee of SiliconPV 2015 under responsibility of PSE AG

Keywords: IBC solar cell; dopant pastes; screen printing;

1. Introduction

IBC solar cells are capable of achieving high efficiency. The concept of the IBC solar cell was first proposed by Lammert and Schwartz in the 1970's [1] and while such cells are being produced commercially [2], wide adoption of this cell structure in the solar industry is hampered by its complexity and high cost. Part of the complexity, in particular, comes from the need to create interdigitated doping patterns on the rear side of the cell, which typically requires multiple additional processing steps compared to standard cells. A number of approaches aimed at reducing the cost of manufacturing an IBC cell have been in development for a number of years, such as ion-implantation [3] or processes using furnace phosphorous and boron diffusions [4].

In this paper, we present an alternative approach which involves using screen printable dopant pastes to create interdigitated doping patterns on the rear side of the cell. In this approach the boron emitter and the phosphorus back surface field (BSF) are created using screen printed boron and phosphorus dopant pastes, respectively. The

Peer review by the scientific conference committee of SiliconPV 2015 under responsibility of PSE AG
doi:10.1016/j.egypro.2015.07.038

phosphorus front surface field (FSF) is created using conventional $POCl_3$ diffusion. This approach is especially attractive due to the simplicity of screen printing, which is already a well-established process in the solar cell industry. Conventional dopant pastes typically suffer from "auto-doping" (i.e. unintentional surface doping outside the paste area) and metal impurity contamination that hurts minority carrier lifetime. Our materials and process are capable of providing interdigitated p and n doping patterns with fine spatial resolution as well as the high bulk lifetimes that are necessary for fabrication of high efficiency IBC cells.

1.1. Conventional dopant paste challenges

Achieving patterned and localized doping using conventional dopant pastes is difficult due to the tendency of such pastes to outgas during the thermal treatments required to drive dopants into the underlying silicon wafer. At typical drive-in temperatures (above 800C) gaseous dopant species are released from the paste regions and are transferred onto non-paste regions as well as onto neighboring wafers. We refer to this effect as auto-doping. Gas phase distribution and auto-doping from phosphorus dopant pastes has been well documented [5-7].

We experienced similar auto-doping challenges with our first attempt at making boron dopant paste as highlighted in Fig. 1. The schematic in Fig. 1 (a) shows gas phase doping from printed paste regions during a quartz tube furnace drive-in. Airborne species from the printed regions are able to reach the non-printed regions of the wafer as well as across to the neighboring wafer. To demonstrate this problem we printed an H-bar test pattern of our first generation boron paste onto a high resistivity (10,000 Ohm-cm) polished wafer and loaded it into the furnace with a bare polished wafer facing it during the thermal drive-in step. The post-drive-in photos in Fig. 1(b) show that the H-bar pattern is no longer distinguishable on the printed wafer (left) and that a brown film has formed on the neighboring wafer (right). Fourier transform infrared (FTIR) spectra were measured at the center of both wafers and are shown in Fig. 1(c). Borosilicate glass (BSG) spectra are clearly observed on both wafers.

Another major challenge for using conventional dopant paste for IBC solar cells is their negative impact on wafer lifetime. It is likely that high impurity levels in the pastes inevitably degrade wafer lifetime during the high temperature treatment required to drive dopants into the wafer. Lifetime degradation of n-type wafers has been reported for both phosphorus and boron dopant pastes with severe degradation reported for boron paste [7]. Studies have also shown that conventional screen-printed phosphorus dopant pastes create more micro-defects in c-Si wafers compared to conventional doping techniques like $POCl_3$ [8].

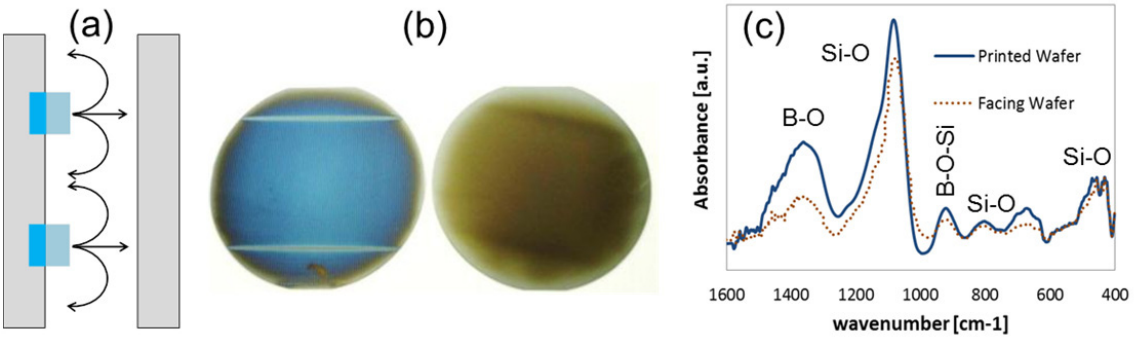

Fig. 1. (a) Schematic of a wafer with a dopant paste pattern facing a bare wafer during thermal drive-in; (b) photos of a boron pate H-pattern printed wafer and its neighboring bare wafer after thermal drive-in; (c) FTIR spectra from the wafers shown in (b) indicating BSG formation on both wafers.

2. Optimized dopant paste approach

2.1. Print fidelity

While the major concerns associated with conventional dopant paste are auto-doping and lifetime degradation, as mentioned above, print fidelity can also be a challenge. Fabricating IBC solar cells with screen printed dopant pastes requires high print resolution in order to align the interdigitated doped pattern. In high-volume solar cell production a screen printable paste must maintain high fidelity between the printed feature and the intended feature size defined by the screen opening. A screen printable paste must behave as a non-Newtonian shear-thinning fluid. A non-Newtonian fluid has flow properties that are not described by a constant value of viscosity. The viscosity of a shear thinning fluid decreases with increasing rate of shear stress. That is, the viscosity of the paste must be relatively low at high shear rates in order to pass through a screen opening, but must be relatively high prior to and after deposition (at low or zero shear rates), in order to not run through the openings while sitting on the screen and not reflow on the substrate surface, respectively. Conventional dopant pastes exhibit near-Newtonian behavior. The viscosity versus shear rate curve for a conventional phosphorus paste is shown in Fig. 2(a). In contrast, our optimized high fidelity phosphorus paste exhibits high viscosity at low shear rates (when paste is at rest) and low viscosity at high sheer rates (during printing). Fig. 2 (b) shows measured line widths for these same two pastes printed with a screen opening of 200 microns. As expected from the flow behavior of these pastes the conventional paste suffers from significant line spreading while the optimized paste exhibits excellent print fidelity.

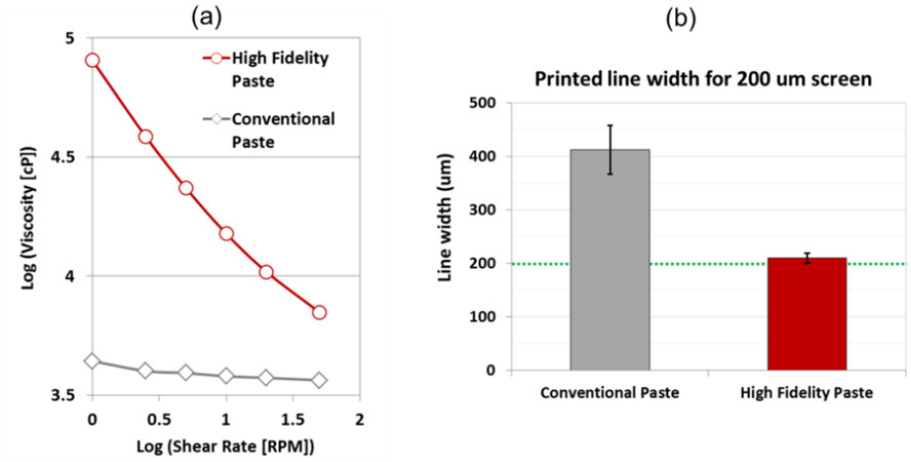

Fig. 2. (a) viscosity versus shear rate for a conventional phosphorus paste and for the high fidelity phosphorus paste used in this work; (b) corresponding printed line widths for a 200 micron screen pattern.

2.2. Doping fidelity

Several formulation and process optimizations were made in order to eliminate auto-doping and achieve localized doping. We are able to demonstrate localized doping both at the micron level and the wafer level. We show here a few examples of localized boron doping followed by an example of localized interdigitated doping.

After printing and thermal drive-in of boron paste emitter line patterns, residual paste is removed from the surface using HF-based wet chemistry. Scanning electron microscopy (SEM) dopant contrast imaging [9, 10] is used to verify localized boron doping by imaging cross-sectional samples at both printed and non-printed regions. Fig. 3(a) is a cross-sectional SEM image from a boron paste printed region. The continuous white band in the SEM image indicates uniform local boron doping. No signs of boron doping are observed in the cross-sectional SEM image from the non-printed region as shown in Fig. 3 (b).

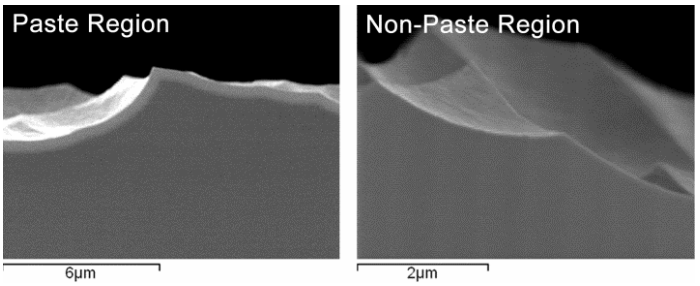

Fig. 3. Cross-sectional SEM images from a boron paste patterned wafer after thermal drive-in and paste strip at a (a) printed region and at a (b) non-printed region.

For large area monitoring across an entire 156mm wafer we employ a selective chemical etch which preferentially etches the undoped regions (the n-type wafer) and does not attack p+ regions. Localized boron doping for an emitter line pattern yields sharply contrasted alternating lines as demonstrated for our process in the photo shown in Fig. 4(a). PL imaging also allows for the verification of localized doping across an entire wafer. Fig. 4(b) shows a PL image of a diffused boron paste emitter line pattern taken after passivation and belt furnace firing.

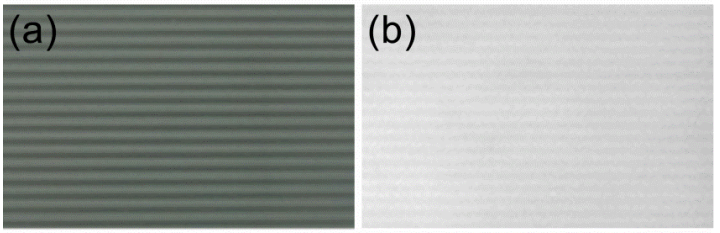

Fig. 4. (a) photo of a boron paste doped pattern after a selective chemical etch; (b) PL image of a boron doped pattern.

Fig. 5 shows secondary ion mass spectroscopy (SIMS) profiles for boron and phosphorous taken in different locations of an interdigitated pattern. Fig. 5(a) shows the adjacent boron and phosphorus doped regions. Fig. 5(b) and (c) clearly demonstrate that the resulting doping is defined by the paste dopant type, with opposite polarity doping suppressed by at least 2 orders of magnitude.

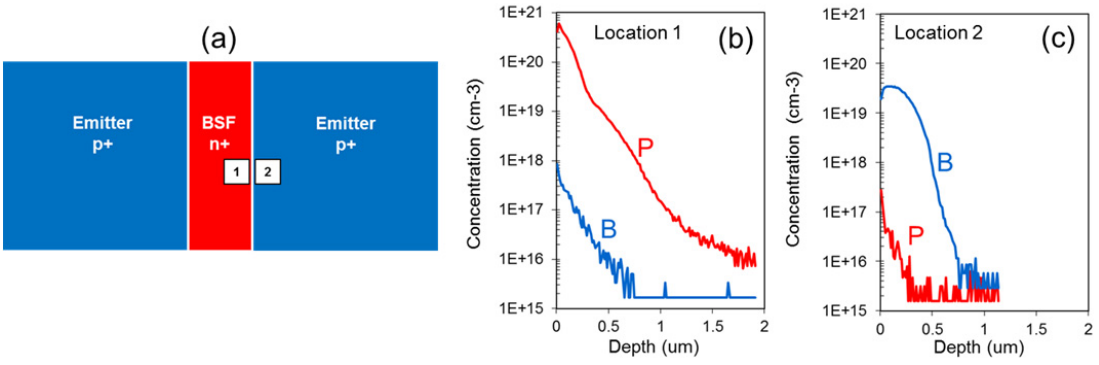

Fig. 5. (a) schematic of an interdigitatd doped pattern with SIMS measurement locations indicated; (b) SIMS profiles for phosphorus and boron at the edge of the BSF region; (c) boron and phosphorus SIMS profiles at the edge of the emitter region.

2.3. Doping capability

Doping strength from our dopant paste is also highly tunable via drive-in conditions. The doping capability of the boron paste is demonstrated with homogeneous p+ diffusions created using a blanket screen print pattern. Fig. 6(a) shows sheet resistance values measured on 156 mm n-type wafers across 25 points for various drive-in conditions. Excellent doping uniformity is demonstrated for all conditions. A sample sheet resistance map is shown in Fig. 6(b).

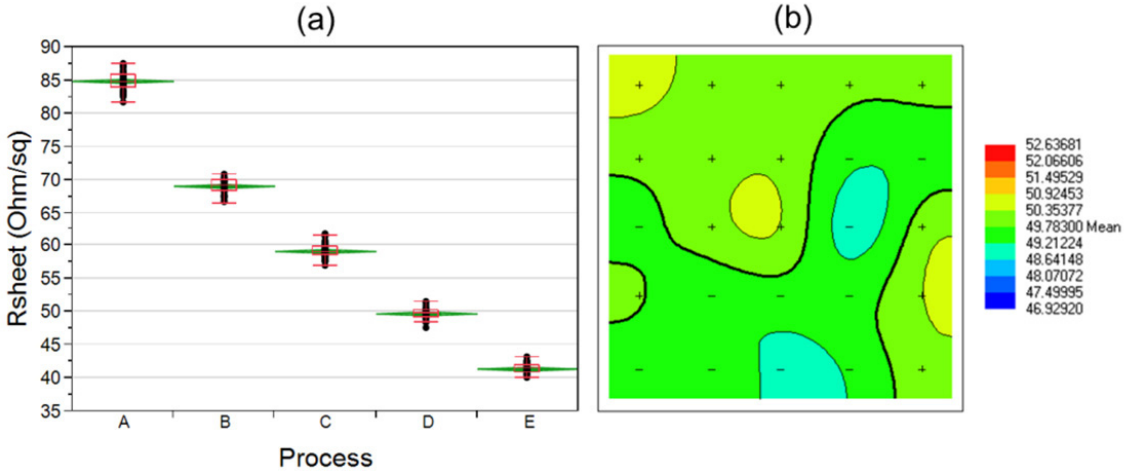

Fig. 6. (a) sheet resistance values on 156mm wafers for homogeneous p+ diffusions created using a screen printed blanket pattern of boron paste varying drive-in conditions; (b) a sample 25 point sheet resistance contour map.

2.4. Recombination

Our doping pastes have been optimized to maintain high bulk lifetime at the end of the IBC cell process. Conventional lifetime measurements which rely on photoconductance have been found to be unreliable on patterned doped structures [11]. As a result, two alternate approaches are used to monitor the wafer lifetime through our IBC process. In order to measure bulk lifetime, all doped regions are chemically etched off and wafers are re-passivated and fired. The measured inverse lifetime curves of such etched back wafers are shown in Fig. 7(a) for samples made using our first generation dopant pastes and our current dopant pastes. Impurity levels have been dramatically reduced to enable bulk lifetime of above 1.5 msec. The implied-V_{oc} of passivated and fired, non-metallized IBC wafers are extracted from calibrated PL images. A series of calibration wafers were prepared with the same geometrical optics (i.e. same wafer thickness, surface texture, and surface passivation) as the IBC wafers. Several homogeneous diffusions of varying strength were applied to the wafers in order to modulate the measured PL counts and qss-PC implied-V_{oc} and to establish a calibration curve. Fig. 7(b) shows a sample PL image of a non-metal IBC wafer. The higher recombination BSF regions are clearly visible in this PL image. The median extracted implied-V_{oc} for our current IBC process is 678 mV.

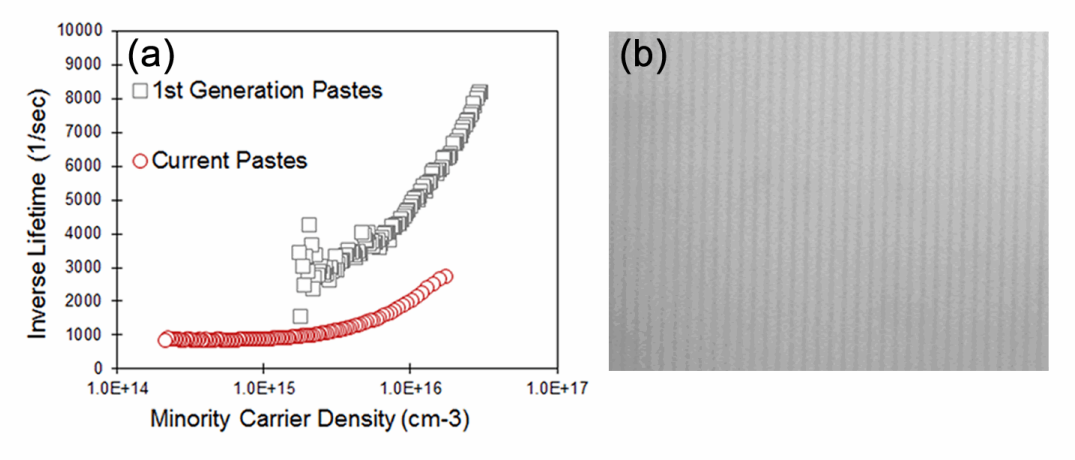

Fig. 7. (a) inverse lifetime curves for IBC wafers with all doped regions etched back; (b) PL image of a non-metal IBC wafer after passivation and firing

The recombination prefactor values for all the doped regions are characterized using homogeneously doped test structures. Table 1 shows the current values for the different doped regions of the IBC cell. Further optimization of the recombination losses in the doped regions are expected to enable implied-V_{oc} values above 680mV.

Table 1. Typical sheet resistance values and recombination prefactor values of the diffused regions

Parameter	Emitter	BSF	FSF
Jo (fA/cm^2)	80	400	25
R□ (Ohm/sq)	55	15	200

3. Solar cell processing

3.1. Process details

IBC cells are fabricated on full area 156 mm n-type pseudo-square CZ-Si wafers. Wafers begin with a random pyramid texture. The FSF is created using a traditional $POCl_3$ doping process. The phosphorus diffusion on the rear side of the wafer is removed using an inline acidic etch process. The rear side interdigitated doping pattern is created using screen printed dopant pastes. The boron emitter pattern is printed and driven in first. Residual paste is removed with an HF-based clean. The phosphorus BSF pattern is printed and driven in last. Wafer edge alignment is used to align the BSF print to the boron emitter. An 80/20 emitter/BSF area ratio is used. After dopant diffusions, the front and the rear sides of the wafers are passivated with SiO_2/SiN_x passivation stacks. The dopant pastes and the process are designed such that the doped regions are visible after passivation enabling subsequent metal alignment steps. Fig. 8(a) shows a BSF test pattern after passivation. Aligned metal contacts to these doped regions are shown in Fig. 8(b), with a zoom-in shown in Fig. 8(c). The alignment of metal fingers to corresponding doped regions is simply achieved using wafer edge alignment. Metals are fired in a standard belt furnace, where contacts are formed through the passivation stack. Busbar-type contacts are used over the fingers, with a screen-printed insulating layer used where required to avoid shunting between opposite polarity contacts.

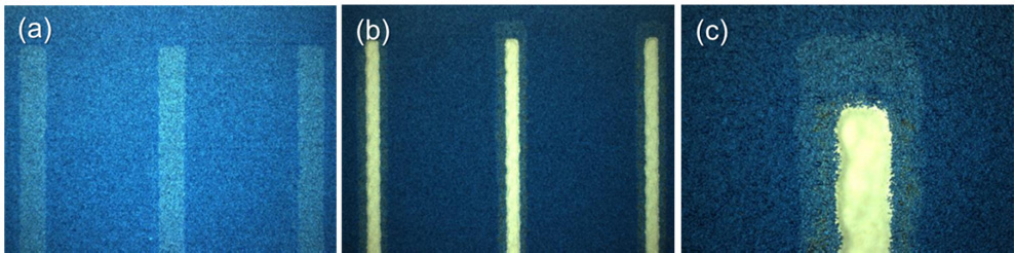

Fig. 8. Optical microscope images: (a) BSF test pattern after passivation; (b) screen printed metal contacts aligned to the visible doped region using wafer edge alignment; (c) zoom-in of a metal contact over a doped region.

3.2. Solar cell results

Screen printed dopant paste 156mm IBC solar cells have been fabricated using only industrial tools. Fig. 9 shows the IV results for a pilot manufacturing run of 100 IBC cells with a peak efficiency of just over 21% and a median efficiency of 20.8%. The bi-modal FF and J_{sc} distributions are due to the varying bulk resistivity of the wafers used in this run. The median values for this run are shown in Table 2.

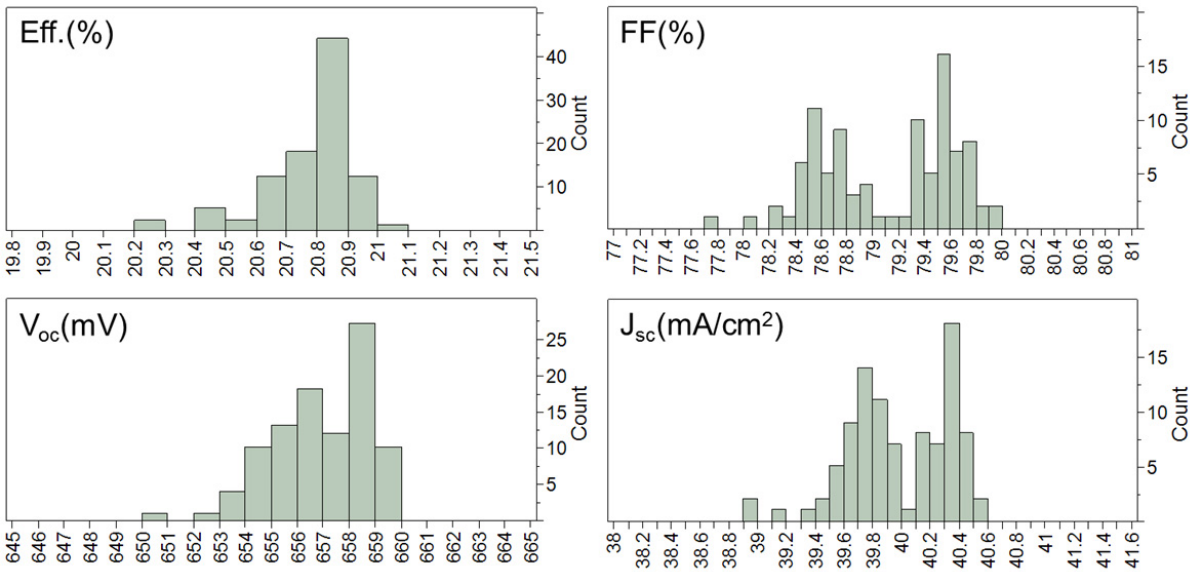

Fig. 9. IV results for 100 all-screen-printed dopant paste 156mm IBC solar cells.

Table 2. Median IV parameter values for 100 all-screen-printed dopant paste 156 mm IBC solar cells.

Parameter	Efficiency (%)	V_{oc} (mV)	J_{sc} (mA/cm^2)	FF(%)
Value	20.8	657	39.9	79.3

4. Conclusions

An alternative approach to fabricating IBC solar cells has been presented where the emitter and BSF regions are created using screen printed dopant pastes and metal contacts are implemented using fire-through screen printed metal pastes. The many challenges associated with using conventional dopant pastes for high efficiency solar cell applications have been overcome. Several improvements were made to our dopant paste formulations and processing in order to achieve high print fidelity, high doping fidelity, excellent doping capability and low impurity levels to maintain high wafer lifetime. Pilot line data for 100 all-screen-printed dopant paste 156mm IBC solar cells made using only industrial tools was presented with a peak efficiency of just over 21% and a median efficiency of 20.8%.

References

[1] Lammert MD, Schwartz RJ. The interdigitated back contact solar cell: A silicon solar cell for use in concentrated sunlight. Electron Devices, IEEE Transactions on. 1977;24:337-42.
[2] Cousins PJ, Smith DD, Hsin-Chiao L, Manning J, Dennis TD, Waldhauer A, et al. Generation 3: Improved performance at lower cost. Photovoltaic Specialists Conference (PVSC), 2010 35th IEEE2010. p. 000275-8.
[3] Bateman N, Sullivan P, Reichel C, Benick J, Hermle M. High quality ion implanted boron emitters in an interdigitated back contact solar cell with 20% efficiency. Energy Procedia. 2011;8:509-14.
[4] Halm A, Mihailetchi VD, Galbiati G, Koduvelikulathu LJ, Roescu R, Comparotto C, et al. The Zebra Cell Concept-Large Area n-Type Interdigitated Back Contact Solar Cells and One-Cell Modules Fabricated Using Standard Industrial Processing Equipment. 27nd EU-PVSEC, Frankfurt, Germany. 2012.
[5] Mouhomb A. Selective emitters for screen printed multicrystalline silicon solar cells. Rev Energ Ren. 2003:83.
[6] Debarge L, Schott M, Muller JC, Monna R. Selective emitter formation with a single screen-printed p-doped paste deposition using out-diffusion in an RTP-step. Solar Energy Materials and Solar Cells. 2002;74:71-5.
[7] Edwards M, Bocking J, Cotter JE, Bennett N. Screen-print selective diffusions for high-efficiency industrial silicon solar cells. Progress in Photovoltaics: Research and Applications. 2008;16:31-45.
[8] Vallejo B, González-Mañas M, Caballero MA. X-ray topography study of monocrystalline silicon wafers diffused with phosphorus by different methods. Appl Phys A. 2013;113:531-6.
[9] Elliott SL, Broom RF, Humphreys CJ. Dopant profiling with the scanning electron microscope—A study of Si. Journal of Applied Physics. 2002;91:9116-22.
[10] Venables D, Jain H, Collins DC. Secondary electron imaging as a two-dimensional dopant profiling technique: Review and update. Journal of Vacuum Science & Technology B. 1998;16:362-6.
[11] Juhl M, Chan C, Abbott MD, Trupke T. Anomalously high lifetimes measured by quasi-steady-state photoconductance in advanced solar cell structures. Applied Physics Letters. 2013;103:243902.